Supporting Information

Wu *et al*. 10.1073/pnas.0811662106

SI Text

Measurement of the Reversal Period. Zhenyu Shi measured 373 reversals of single cells that were visible at the edge of the swarm from Movie S1. The distribution of their reversal periods is shown in Fig. S1. The distribution is uni-modal and asymmetrical with an average of 8.8 ± 2.1 min. Most cells have reversal periods between 5–11 min.

Correlation Function and the Calculation of Correlation Distance. We use the following correlation function (discrete and 2-D form of the one used in eq [1]) to compare levels of alignment of cells in swarms with different cell reversal periods:

$$C(r) = \frac{1}{N(r)} \sum_{\substack{i,j \\ i \neq j}}^{N(r)} (2\cos^2\theta_{ij} - 1) \qquad [S1]$$

Here θ_{ij} denotes the angle between the orientations of the i-th and j-th cells (the orientation of a cell is defined as the direction from its the tail node to its head node); r is the distance between a pair of cells and $N(r)$ is the number of cell pairs separated by a distance r.

The correlation distance, l, is defined as the distance beyond which $C(r)$ no longer depends on distance, having reached its background level. Ideally, the point where $C(r)$ becomes constant should be taken as a correlation distance. In practice this point is difficult to determine because of the stochastic fluctuations arising from the finite number of cells simulated. After the horizontal tail of $C(r)$ had been approximated, the MEAN and its standard deviation (SD) were determined for the data points scattered along the tail. The point at which $C(r)$ first fell within the zone defined by the MEAN ± SD was taken for the correlation distance. Statistically stable values of l were thereby obtained.

Detailed Description of the Computational Model. The cell-based computational model for *M. xanthus* has been described in detail in the preceding paragraph. It is a two-dimensional stochastic and off-lattice model. Cells are initially distributed in a 333 μm by 100 μm domain at a density of 50 K-S units (similar to Fig. 5). At this density the cells cover about half the surface of the domain. The number of cells in that domain is returned to its initial value after each movement, to enforce the steady state. The positions of distributed cells are randomly selected, whereas the orientations of cells are taken to be distributed symmetrically around the radial direction, because as the cells grow the swarm has radial symmetry as it expands. On these assumptions, we choose the distribution function to be $f(x) = (6/\pi^3)x(\pi - x)$.

Each cell is represented by a string of N nodes. The relative positions of the nodes are allowed to change, so that the cell body can bend or elongate. One cell consists of (N-1) flexible segments of length r each. There are (N-2) angles θ_i between neighboring segments. For each cell we define a configuration energy function (see ref. 2) to keep the cell shape relatively stable. We have chosen to set $n = 3$, so that every cell consists of two segments, which is required minimally for cell bending.

For simplicity, we use the velocity of the head-node to lead the entire cell forward. The head speed is fixed for each simulation, usually at 4 microns/minute. The velocity direction is determined in the model by considering *S* motility, *A* motility, slime trails, and cell–cell interactions. A motility pushes the cell in the direction of its long axis, led by the head. *S* motility, by using type IV pili at the leading end, pulls the cell toward the average orientation of the cells ahead. Cells also turn to follow a slime trail that they cross. We define a two dimensional slime vector field that records the slime trail orientation at a given position. The equations describing these effects are given in ref. 2.

After the head node moves, the other 2 nodes will then move to new tentative positions that would keep the cell length and shape constant. Such tentative movements will be accepted or rejected according to the changes of configuration energy function by using Metropolis algorithm (3). Tentative movements are not taken at random, rather they are made in preferred directions with small deviations allowed. The tail node tends to move along the direction pointing from itself to the middle node, whereas the middle node moves in the direction from tail to head node. These settings generate average bending of cells in good agreement with the experimental data in (4). *M. xanthus* cells are observed to bend on average at an angle of 15° with the standard deviation of 13° during a move of 1.33 cell length (4). The model yields a mean bending angle of 15–16° with the standard deviation of 12–13° during a continuous move of 1.33 cell lengths.

In the model, each cell reverses after the fixed time T, the reversal period. Each cell has its own reversal clock that marks time from 0 to T, and T can be adjusted from one simulation to another. Initially, the clocks are set to random phases between 0 and T. Then, at each time step in a simulation, the phases increase by 1 unit. When the phase reaches T, the cell reverses: The cell exchanges the position of its head and tail; it resets its own clock to zero, remains motionless for 1 min while the engines are exchanged, and finally it moves off in the reverse direction.

At each time step we first check the reversal clock to see whether it is time to reverse the cell's polarity. Then the direction that the head should move is computed. If the computed location is unoccupied, the head node moves forward at the fixed speed. If there would be a collision with another cell, it is resolved by using the algorithm described in (2). After moving the head node to a new position, the positions of the other 2 nodes is updated appropriately. After all cells have moved, the number of cells which have moved across the outer boundary into the free space is calculated, and an equal number of cells is added to the simulation domain to maintain their number constant. Fig. S2 shows typical simulation images at the beginning (*A*) and after 200 min (*B*). *B* can be compared with the experimental pictures in Fig. 1 in the main text in terms of cell clustering.

Time Duration of Simulation Runs. Each simulation was run for 1,000 time steps, which is equivalent to 200 min of experimental swarming. This duration corresponds to the experimental Movie S1. Because the swarm expansion rates of both WT and frz mutants are observed to be constant over the 4-h period of the movie, we maintain the cell density constant (Fig. S2*A*). In this way the rate of swarm expansion (proportional to the cell flux) is almost constant after 50 min (Fig. S3).

Reproducibility and Stability of Simulation Results *Unidirectional cells reduce swarming efficiency of A⁺S⁻ mutant.* As shown in Fig. 2 of main text, the cell flux decreases gradually as the proportion of unidirectional (nonreversing) cells in a mixed population of A^+S^+ cells is increased in simulations. Such decreases are also observed for an A^+S^- mutant (Fig. S4). The average flux of 10 independent runs is plotted against the proportion of unidirectional cells in the mixture. Unidirectional cells were randomly

distributed within the initial area of cells (Fig. S2*A*). A reversal period of 8 min was used for these A^+S^- mixtures.

The optimal reversal period of A^+S^- mutant depends on the cell speed. The optimal reversal period of A^+S^+ cells depends on the cell speed (Fig. 4 of main text). Similar behavior can be seen for A^+S^- mutant, as shown in Fig. S5. The red curves are reconstructed from the data of normal speed (4 μm/min), by using the functions $Y = C1 * f(2x)$ for 8 μm/min and $Y = C2 * f(x/2)$ for 2 μm/min respectively to show the effect of scale change. Here x is the reversal period, $f(x)$ is the fitted function for the original curve of normal speed, and $C1$ and $C2$ are constant factors dependent on the average speed.

Noise in the reversal period should have little effect on the cell fluxes. We investigated how fluctuations in the reversal period might be expected to affect the simulations, considering that the reversal period was a constant in each simulation. However, the reversal periods of the cells at the edge of a swarm are observed to have the uni-modal distribution that is shown in Fig. S1. To see what effect fluctuations in period might have throughout the swarm, we considered reversals to be distributed with an average value plus zero-mean Gaussian noise. We used such distributions in the simulations with average periods of 4, 8, and 20 min, and for both wild-type and an A^+S^- mutant. Over a wide range of noise levels (standard deviations), we observed little, if any change in the cell fluxes, as shown in Fig. S6.

The optimal reversal period is stable to variations in model parameters. We investigated the stability of simulation results to variations in the model parameters that set the relative strengths of S-motility, A-motility, and slime trails in determining the velocity direction, as described in *Detailed Description of the Computational Model*. For the simulations described in the text we used parameter values of 0.5:1:2 (for the wild-type), and 0:1:2 (for the A^+S^- mutant) to give a 2-fold difference in swarming efficiency that is observed between wild-type and A^+S^- mutant as described in ref. 2. How might the choice of parameter values affect the optimum range of reversal periods obtained in Fig. 3? Quantifying that range is an important feature of this work. Because the velocity direction is a unit vector, we can fix the contribution of A-motility as 1, and vary the other two parameters subject to the constraint of retaining a 2-fold difference between the average cell flux of wild-type and the A^+S^- mutant. As shown for wildtype cells in Fig. S7, when the S-motility parameter is 0.25, 0.5, and 0.75, the slime-cell interaction strength must be $\approx$0.65, 2.0, and 3.0 respectively to produce the 2-fold difference in cell flux between wild-type and A^+S^- cells. Therefore, in addition to 0.5:1:2 as used in the original simulations, parameter combinations 0.25:1.0:0.65 and 0.75:1.0:3.0 were tried. We calculated the average cell fluxes of wild-type swarms at various reversal periods for the three parameter combinations, and observed that the optimum range of reversal periods remained stable at 8 $\pm$ 3 min for those parameter combinations like the original set (Fig. S8).

Returning to Fig. S7, little, if any cell flux variation is seen for the A^+S^- mutant as the strength of the slime-cell interactions is varied from 0.5–5. Thus the A^+S^- mutant would also have the same optimum range of reversal period for all of the slime-cell interaction parameters tested.

Swarming Efficiency Depends on Cell Shape (Aspect Ratio). In all simulations presented in the text we used the experimentally observed aspect ratio of *M. xanthus* cells, $\approx$10:1. To test the effect of different aspect ratios, we modified our model so that the aspect ratio can be changed to any precise value. Although the modification leads to smaller cell flux for a given reversal period, it does not affect the 2-fold difference between the swarming efficiencies of wild-type and A^+S^- mutant. We used the model to test the effect of cell shape on swarming. As shown in Fig. S9, the swarming efficiency decreases as the aspect ratio

decrease from 10:1 to 2:1. This confirms the importance of an elongated shape for the swarming of *M. xanthus* cells.

Measuring the Swarm Expansion Rates of DZ2 and the Frz Mutants. A CTT 1% agar plate (5) was inoculated in the center by stabbing with a round toothpick that had been loaded with a small amount of the bacterial strain to be tested, and incubated at room temperature (22–23 °C). The bacteria swarmed up the sides of the perforation in the agar, then spread over the surface of the agar as a circular disk. Each day, for 2–3 weeks, the diameter of the swarm was measured along the same line, by using a straight-edged rule. DZ2 and DK1622 wild-type strains and their frizzy, A-motility and S-motility mutants yield straight lines when diameter is plotted against time. The slopes of the lines, the swarm expansion rates, characterize the mutants. Usually, two swarms of the same strain on separate plates were measured and their data plotted together to obtain the slopes that were reported in Table 1.

To describe the behavior of deletion mutants that lack a frizzilator, and have a time between reversals of 34.1 min (32), we assume that the average cell behaves as follows:

1. It moves in one direction for 5 min, then stops for 29 min.
2. After 34 min, MglAB switches.
3. The cell reverses, moving in the reverse direction for 5 min, then stopping for 29, etc.

Evidence that the A Engines are Polar and Not Lateral. The evidence for polar A engines has been reviewed (10). Recently, the AglZ protein was observed to form transient focal clusters at 2 μm intervals in the front half of moving *M. xanthus* cells (6). The clusters remain fixed in position with respect to the agar substrate, as the cell body moves forward. AglZ is a filament-forming coiled-coil protein that is required for A motility, but not required for S motility (7). The focal adhesions would be forming within the capsular slime gel, and would provide rigid, but transient connections between AglZ filaments, possibly in the periplasm, and the agar substrate. Focal adhesions could play an essential role in the mechanics of propulsion by slime secretion. Consider a cell that is gliding on its layer of capsular slime, which is the interface between the cell's lipopolysaccharide and the agar substrate. As that cell is pushed forward by slime secretion from its lagging end, elastic stress would be created in the slime layer, and that stress would oppose the cell's forward motion, as discussed by Purcell (8). Periodic focal adhesions might allow the stress accumulated between two adhesion sites to be dissipated by diffusion of the capsular polysaccharide and lipopolysaccharide molecules. As the polysaccharide chains relaxed to unstressed conformations, the stress energy would be dissipated as heat. Without dissipating that energy, forward motion due to polar slime secretion would slow or stop under these conditions of low Reynolds number where viscous forces dominate and momentum plays no role (8, 9). Thus, focal adhesions are more likely to be sites of energy dissipation, rather than sites at which translational energy is injected as suggested by Mignot (6). Translation of *M. xanthus* at low Reynolds number can be obtained either by pulling with type IV pili and breaking the adhesions; or by polarized secretion of propulsive slime, which is chemically the same as capsular slime but is strictly oriented by the dense, polar array of nozzles.

Mignot elaborated on the focal adhesions by suggesting that each was associated with some as yet uncharacterized motor that propelled the cell forward (6). Not only is there no need for another engine, as just pointed out, but Mignot's model has several unresolved difficulties. Because the focal adhesion sites appear to lie on a helix (6), the cell would be expected to rotate about its long axis as it progressed over the substratum. But rotation has not been demonstrated, and there are several indications against rotation. First, many of Mignot's images show
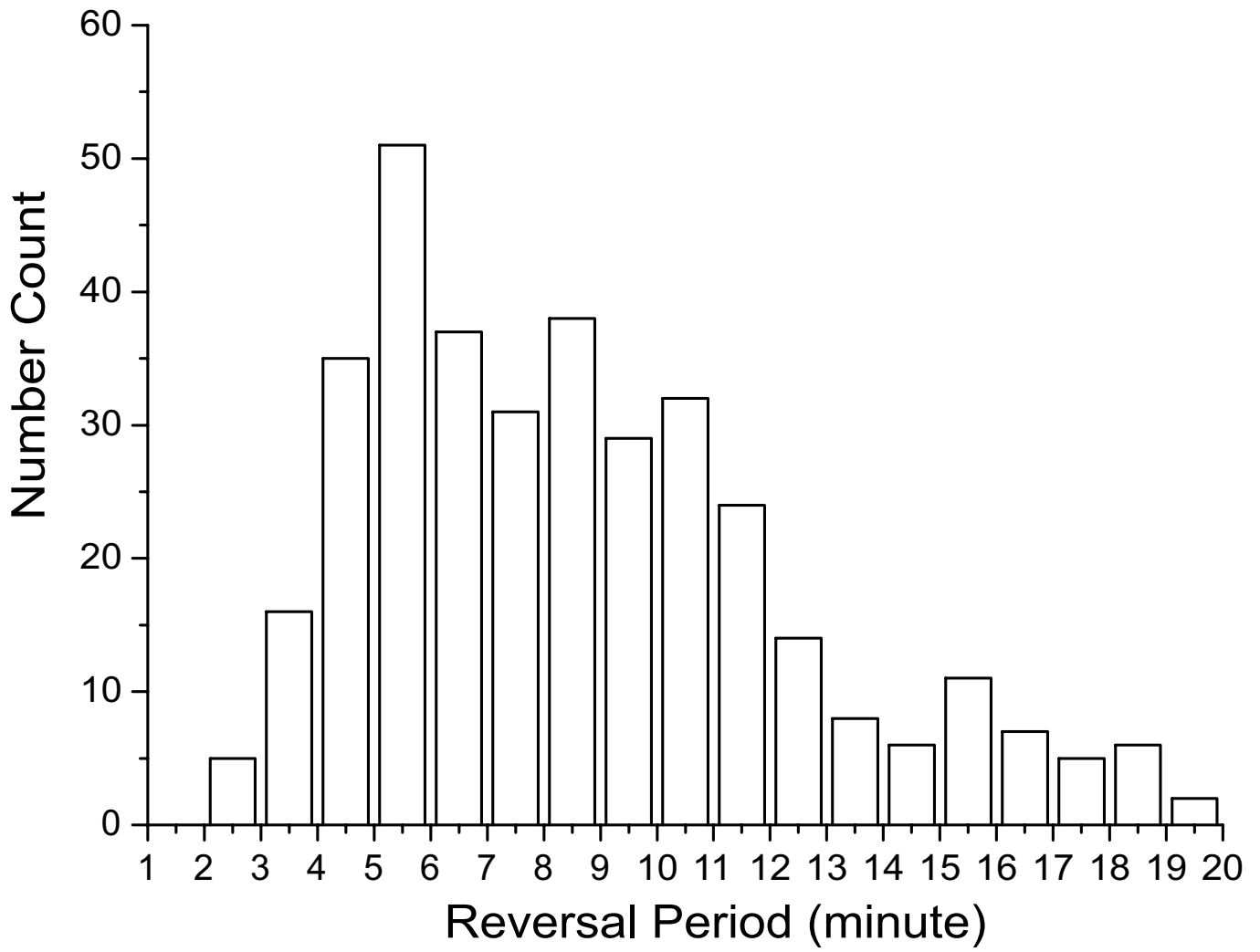
bent cells. Rotation of a bent cell around its long axis would either require the cell to straighten out by sliding to the side, or to break one or more of the adhesions; neither is observed. Second, Hans Reichenbach has published movies of several different myxobacteria in the process of gliding (11, 12, 13), and a few of his cells had cytoplasmic inclusions, possibly glycogen grains. If the cells were rotating about their long axis, the inclusions should have appeared to oscillate across the width of the cell, but they did not. Third, *M. xanthus* cells extend several type IV pili forward. If two pili from the same cell were to attach to cells ahead, and those pili were to retract, cell rotation would be opposed by the pulling of the pili. Thus, the adhesion motor model of A motility (6) predicts that A and S motility should compete with each other. Instead it was shown that the two engines actually help each other (4). Finally, the adhesion motor model (6) neglects the problem as to how the adhesion motor complexes would incorporate information as to which particular direction the cell was moving, i.e., which of its poles was leading. Filaments of the AglZ protein, which define an adhesion site (6) can form striated arrays indicating that the filaments are in register (7). Yet, there is no evidence for a polarity in that alignment that would reflect the gliding direction. For example, evidence for AglZ localization to two helices differing in hand is lacking. Considering these deficiencies, there is no reason to accept Mignot's proposal that motors are associated with the adhesion complexes (6). For the reasons suggested, adhesion complexes could facilitate A motility propelled by polar slime secretion.

1. Saintillan D, Shelley MJ (2007) Orientational order and instabilities in suspensions of self-locomoting rods. *Phys Rev Lett* 99:058102.
2. Wu Y, Jiang Y, Kaiser D, Alber M (2007) Social interactions in myxobacterial swarming. *PLoS Comput Biol* 3:e253.
3. Newman MEJ, Barkema GT (1999) in *Monte Carlo Methods in Statistical Physics* (Clarendon Press, Oxford) pp 46–53.
4. Kaiser D, Crosby C (1983) Cell movement and its coordination in swarms of Myxococcus xanthus. *Cell Motil* 3:227–245.
5. Yu R, Kaiser D (2007) Gliding motility and polarized slime secretion. *Mol Microbiol* 63:454–467.
6. Mignot T, Shaevitz JW, Hartzell PL, Zusman DR (2007) Evidence that focal adhesion complexes power bacterial gliding motility. *Science* 315:853–856.
7. Yang R, *et al*. (2004) AglZ is a filament-forming coiled-coil protein required for adventurous gliding motility of *Myxococcus xanthus*. *J Bacteriol* 186:6168–6178.
8. Purcell EM (1977) Life at low Reynolds number. *Am J Phys* 45:3–11.
9. Wolgemuth CW (2005) Force and flexibility of flailing myxobacteria. *Biophys J* 89:945–950.
10. Kaiser D (2008) *Myxococcus*—from single-cell polarity to complex multicellular patterns. *Ann Rev Genet* 42:110807.091615.
11. Reichenbach H (1968) *Archangium violaceum (Myxobacteriales) Schwarmentwicklung und bildung von protocysten* Film E 777/1965 (Institut fur den Wissenschaftlichen Film, Gottingen, Germany). 16 mm, black and white, 11 min at 24 frames/sec.
12. Reichenbach H (1966) *Myxoccoccus spp. (Myxobacterales)* Schwarmentwicklung und Bildung von Protocysten Film E778/1965 (Institut fur den Wissenschaftlichen Film, Gottingen, Germany). 16 mm, black and white, 14 1/2 min at 24 frames/sec.
13. Reichenbach H (1974) *Chondromyces apiculatus (Myxobacteriales) Schwarmentwicklung und morphogenese*. Film E 779/1965 (Institut fur den Wissenschaftlichen Film, Gottingen, Germany). 16 mm, black and white, 15 min at 24 frames/sec.
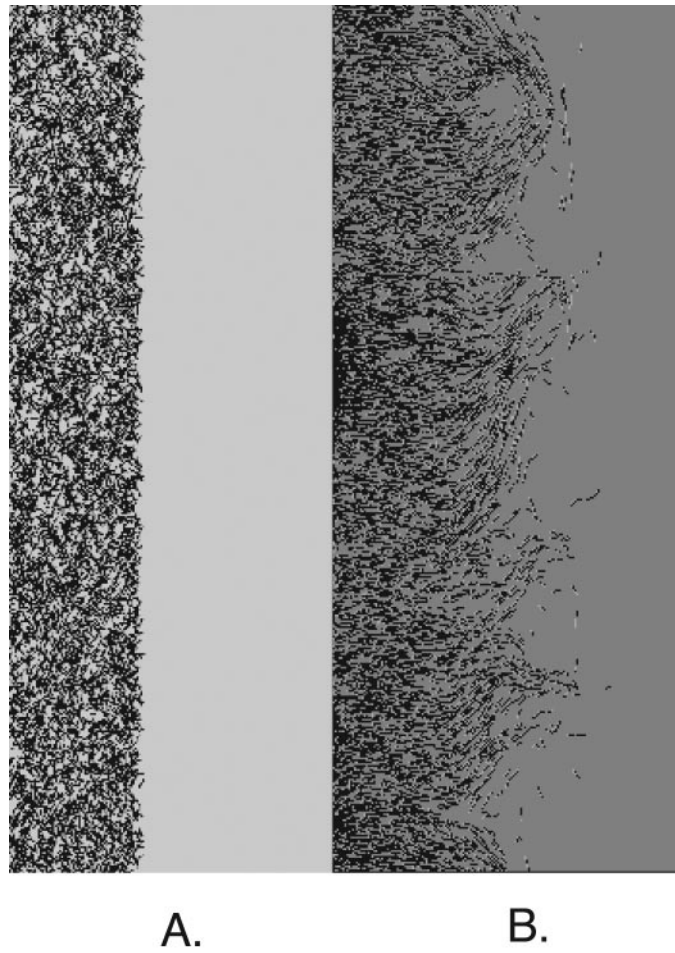
Fig. S1. The statistics of reversal period data.

Fig. S2. Simulation images. (*A*) At the beginning of simulation, cells are distributed in a region referred to as the initial swarming domain. (*B*) After 200 min simulation (wild-type).
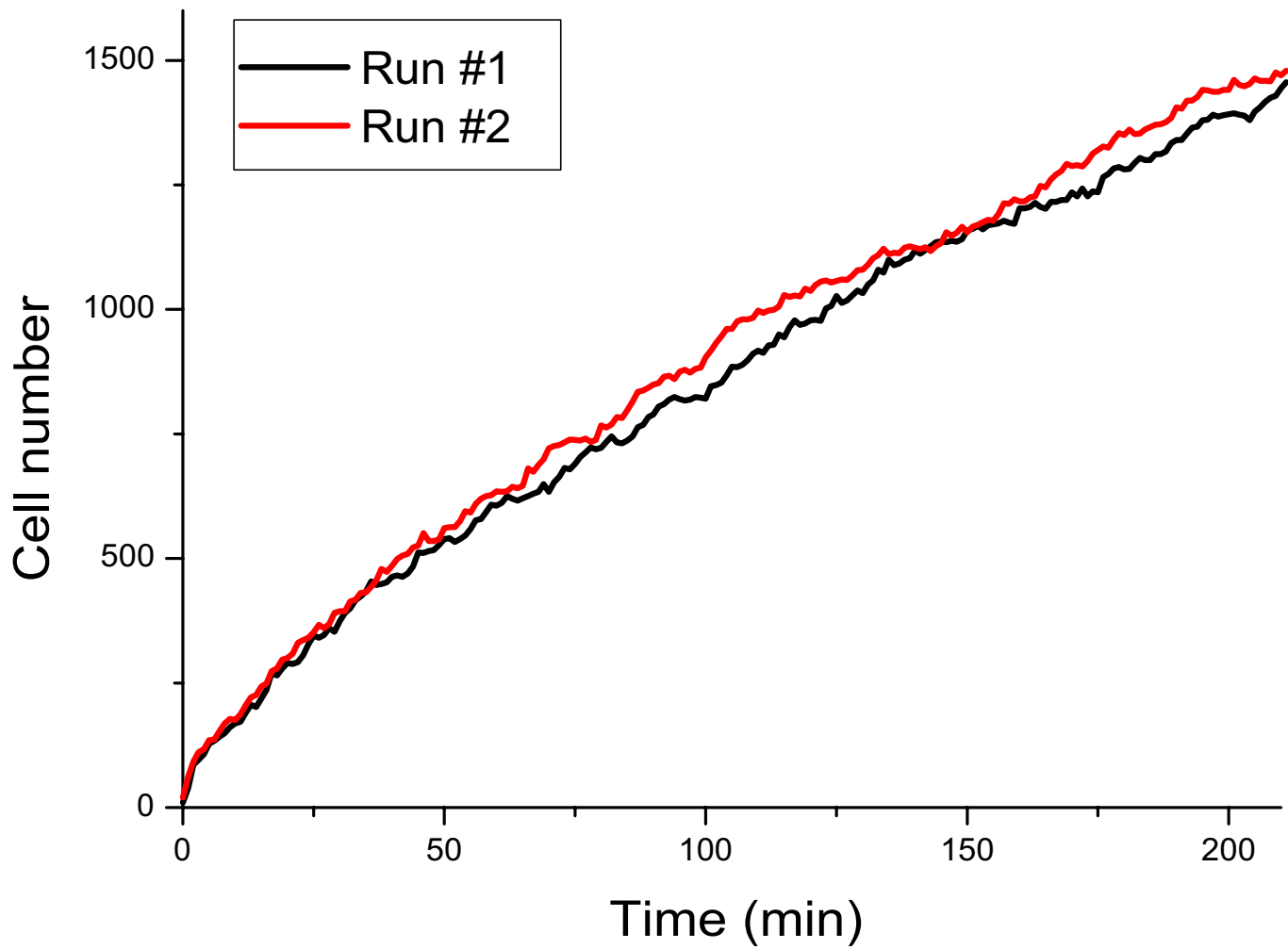
Fig. S3. The number of cells that cross out of the swarming edge is plotted against time for a simulation of 200 min (2 independent runs).
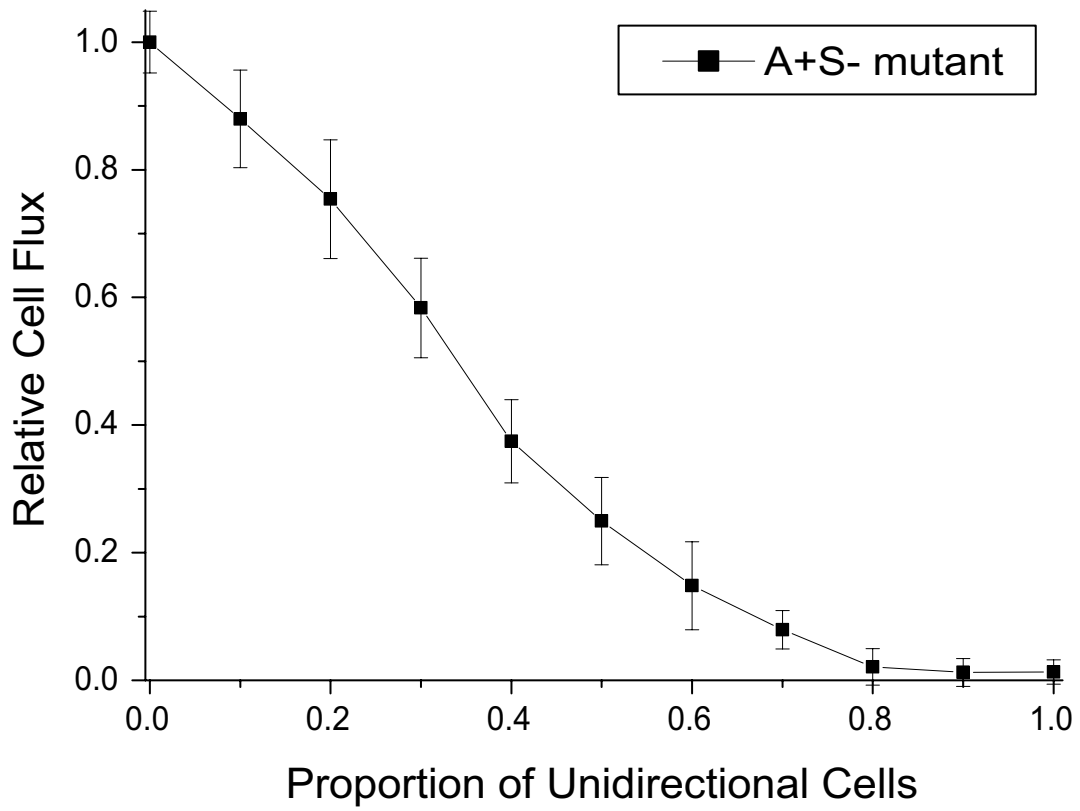
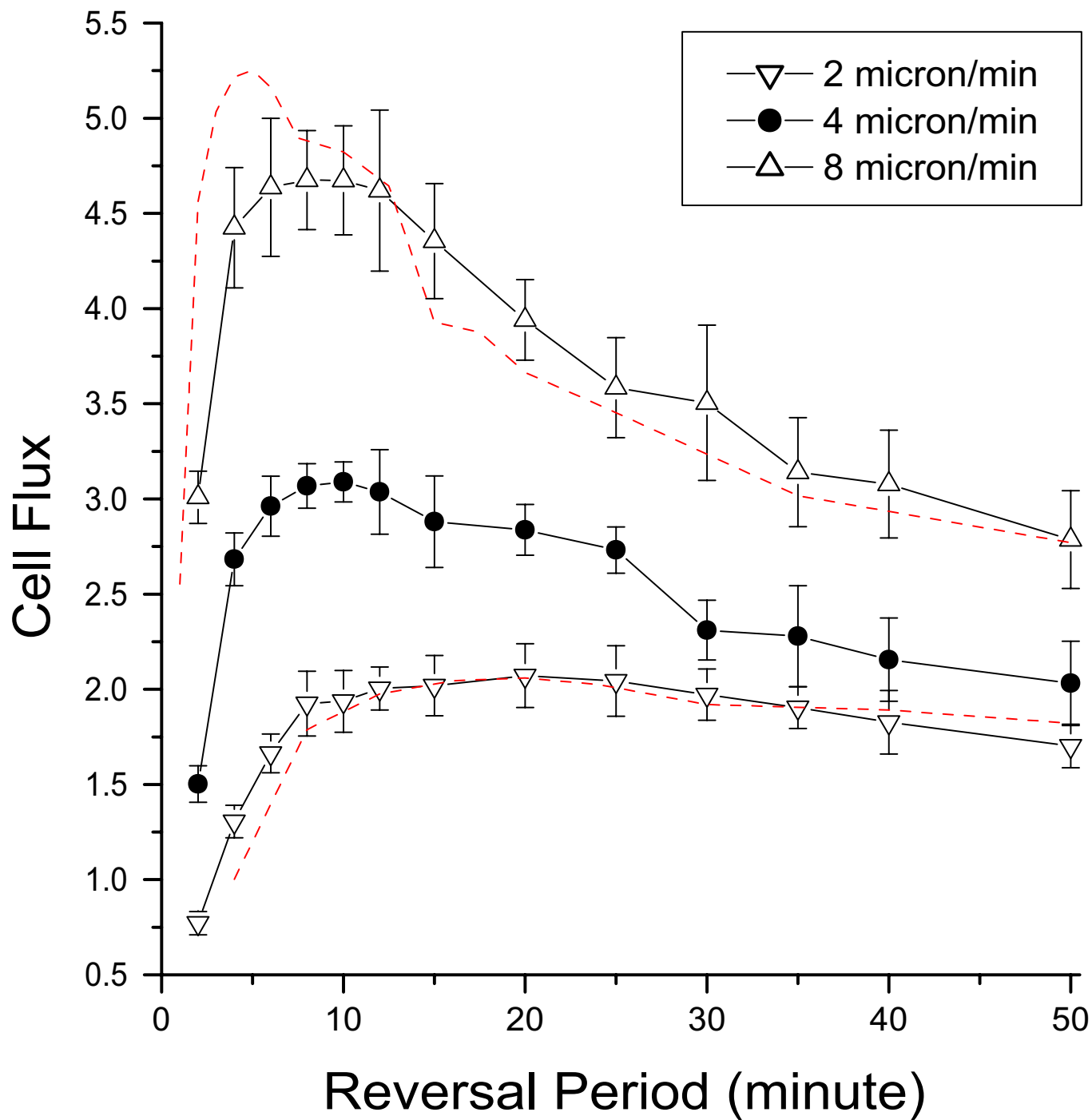**Fig. S4.** Dependence of the flux on the proportion of unidirectional cells in A$^+$S$^-$ mixtures.

Fig. S5. Dependence of the optimal reversal period of A⁺S⁻ mutant on the cell speed.
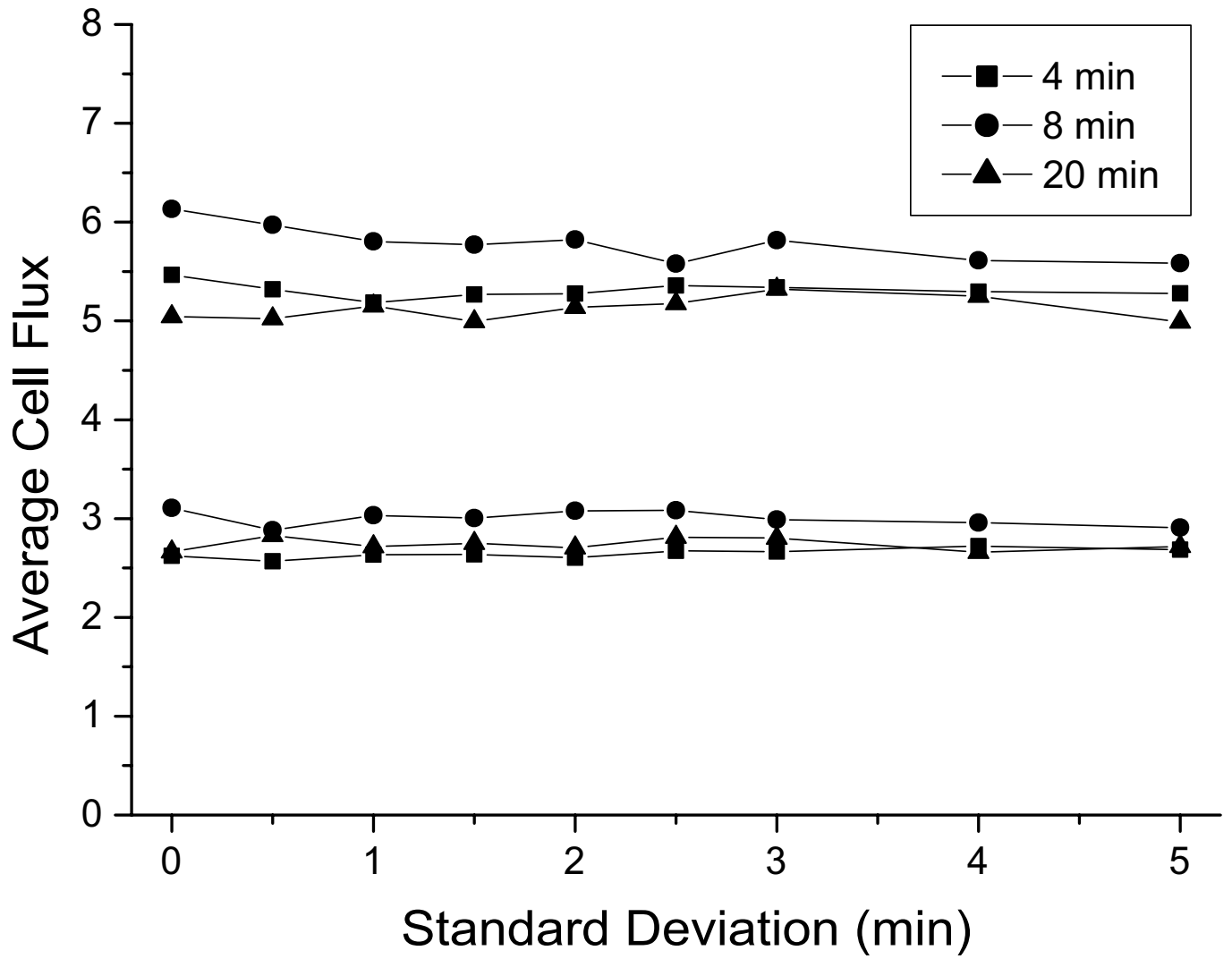
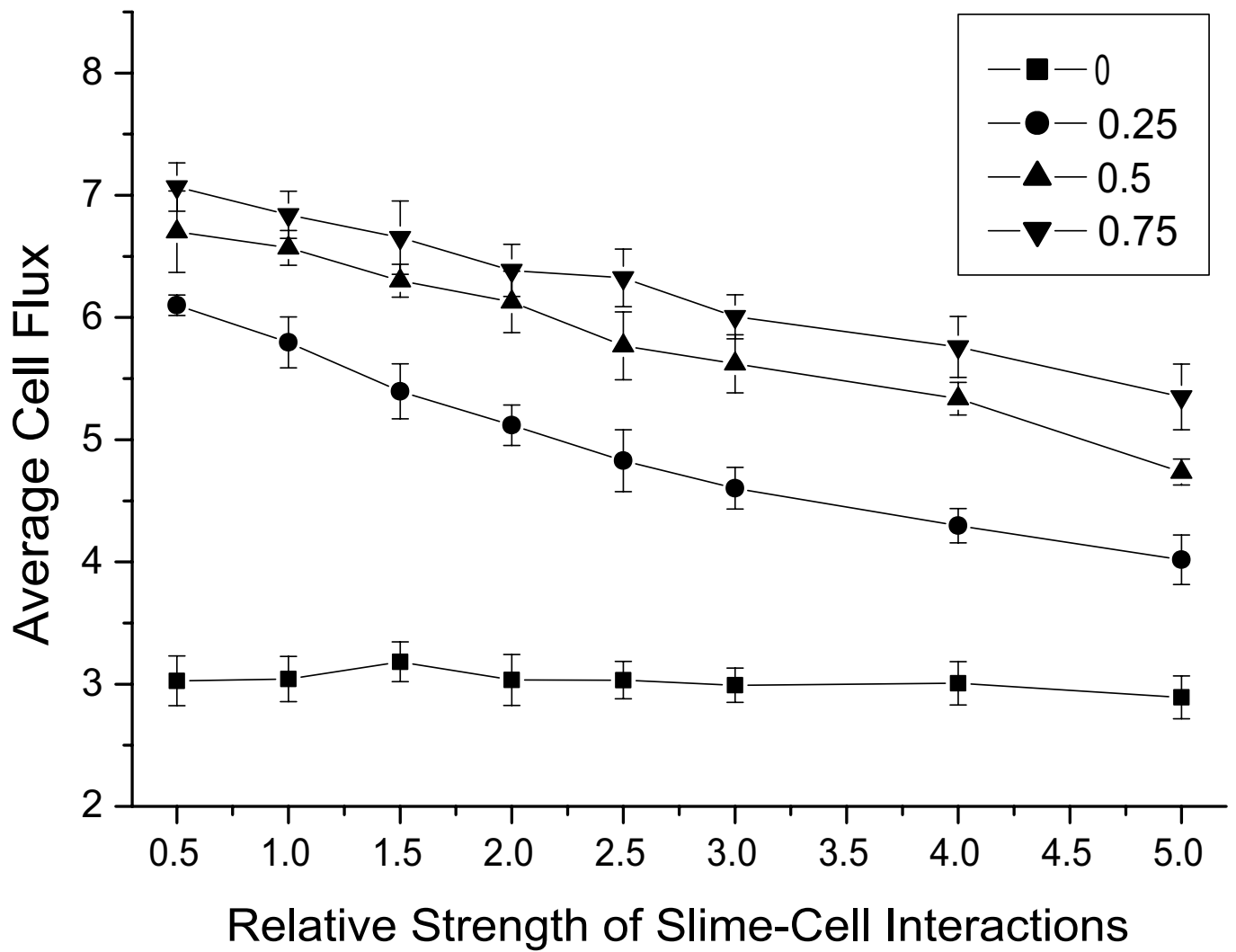**Fig. S6.** The average cell fluxes at various noise levels of reversal period distribution.

Fig. S7. The dependence of average cell flux on slime-cell interactions at different S-motility strengths. Different colors and symbols represent different strengths of S-motility effect, changing from 0, 0.25, 0.5, to 0.75. The black curve with zero S-motility strength is the A^+S^- mutant.
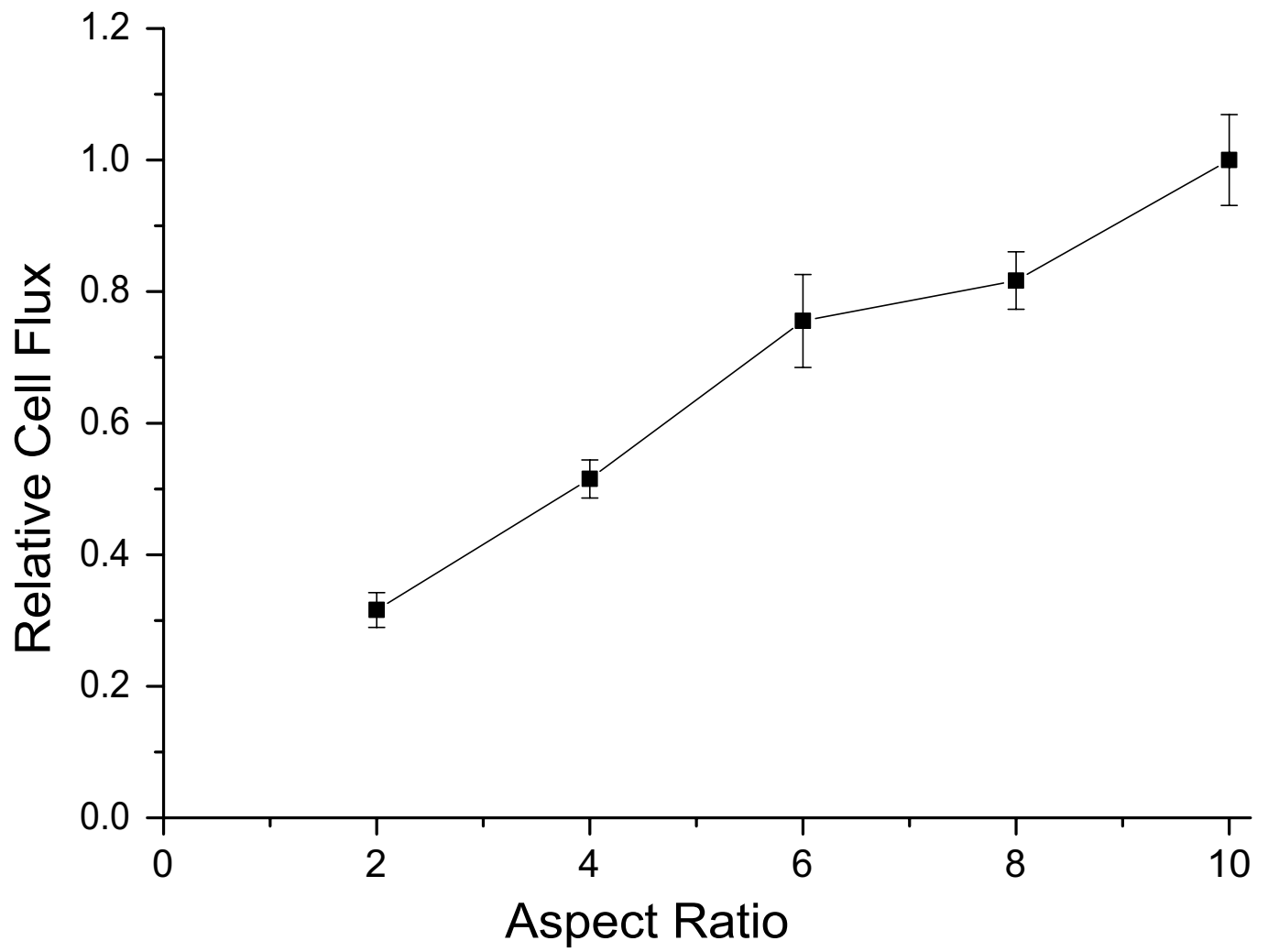
Fig. S8. The average cell flux of wildtype swarms as a function of reversal period for 3 parameter settings.
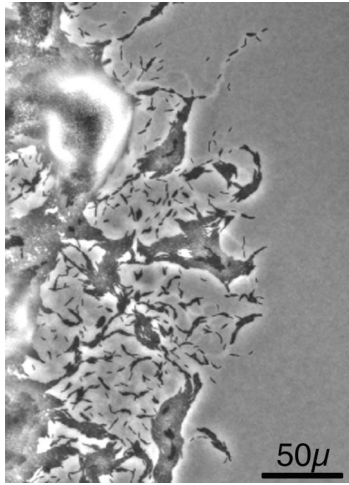
Fig. S9. The relative cell flux to the wild-type value (12.83 cells per min per ml of edge's cross-section) is plotted against different aspect ratios.

Movie S1. Still of first frame, showing the distribution and orientation of cells at the swarm edge. In addition to individual cells, multicellular rafts and multicellular mounds are evident. The swarm is expanding in the radial direction, which is to the right in this image. A 50μ scale bar is shown at the lower right. For the movie, an image was collected with a 20x objective lens every 30 sec for 3 hrs.

Movie S1 (AVI)